

# Single-Shot Carrier-Envelope Phase Determination of Long Superintense Laser Pulses

Jian-Xing Li,<sup>1,2,\*</sup> Yue-Yue Chen,<sup>1</sup> Karen Z. Hatsagortsyan,<sup>1,†</sup> and Christoph H. Keitel<sup>1</sup>

<sup>1</sup>Max-Planck-Institut für Kernphysik, Saupfercheckweg 1, 69117 Heidelberg, Germany

<sup>2</sup>School of Science, Xi'an Jiaotong University, Xi'an 710049, China



(Received 3 July 2017; published 23 March 2018)

The impact of the carrier-envelope phase (CEP) of an intense multicycle laser pulse on the radiation of an electron beam during nonlinear Compton scattering is investigated. We have identified a CEP effect specific to the ultrarelativistic regime. When the electron beam counterpropagates with the laser pulse, pronounced high-energy x-ray double peaks emerge near the backward direction relative to the initial electron motion. This is achieved in the relativistic interaction domain, where both the electron energy is required to be lower than for the electron reflection condition at the laser peak and the stochasticity effects in the photon emission need to be weak. The asymmetry parameter of the double peaks in the angular radiation distribution is shown to serve as a sensitive measure for the CEP of up to 10-cycle long laser pulses and can be applied for the characterization of extremely strong laser pulses in present and near future laser facilities.

DOI: 10.1103/PhysRevLett.120.124803

Superintense laser techniques have been developing rapidly in recent years [1–4], opening bright prospects for the investigation of new regimes of laser-matter interaction [5–9]. Extremely intense lasers require new techniques for the characterization of laser-pulse parameters: intensity, focal radius, pulse shape, chirp, and carrier-envelope phase (CEP). The CEP is an important parameter in strong field physics and nonlinear QED. Thus, the CEP has a significant impact on the electron spin [10], the angular distribution, asymmetry, and the cross section of nonlinear Compton scattering [11–13], of the electron-positron pair production process [14–19], and provides a useful handle to control the physical properties of laser-matter interaction. Commonly, the CEP effects arise from the spatial asymmetry of few-cycle laser pulses. When the laser intensity is below the relativistic threshold ( $I \sim 10^{18}$  W/cm<sup>2</sup>), the CEP can be determined via asymmetry of above-threshold ionization (stereo-ATI) [20–22], or probing the field with  $f - 2f$  interferometry [23,24], or with the streaking method [25], or with terahertz-emission spectroscopy [26]. In the relativistic domain of laser intensities, it was shown that signatures of the CEP of few-cycle laser pulses (up to at most two cycles) can be detected via nonlinear Compton scattering from either the bandwidth of the angular distribution of the electron radiation [12] or the differential cross sections of the Breit-Wheeler pair production process [17]. However, ultraintense laser pulses, with intensities  $I \sim 10^{22} - 10^{25}$  W/cm<sup>2</sup>, commonly consist of about 6–10 cycles (pulse duration  $\sim 20$ –30 fs) [1–4,27]. Moreover, there are indications that in the ultrarelativistic regime the characters of CEP effects may change, which may emerge even in multicycle laser pulses. For instance, the phase properties of the harmonics generated at the laser-plasma interface have been shown to be coherently controlled through the phase of

the long driving laser pulse [28]. Thus, there is an apparent need for novel methods to precisely characterize the CEP for multicycle ultraintense lasers.

In this Letter, we present a CEP effect of an intense multicycle laser pulse in the angle-resolved radiation spectra of an electron beam via nonlinear Compton scattering in the ultrarelativistic regime. A relativistic electron beam initially counterpropagates with the laser pulse, see Fig. 1. We choose the regime when the backward radiation relative to the electron's initial motion is enhanced, forming a broad peak splitting into two parts.

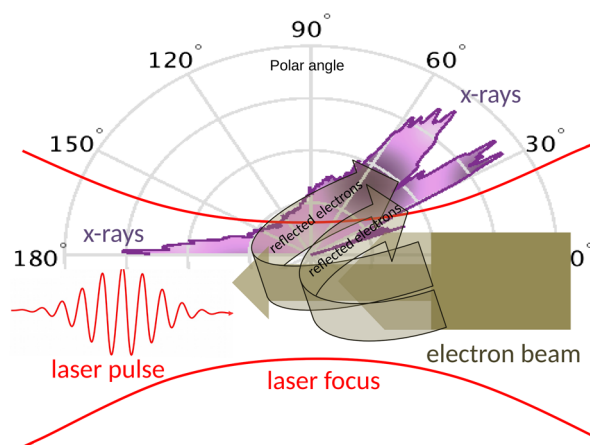


FIG. 1. Interaction scheme where the focused laser and the electron beam counterpropagate. For  $\gamma \ll \xi$ , parts of the electron beam are reflected, escape from the laser cycles, and emit x rays at different laser angles in backward direction. Two backward x-ray peaks are sensitive to the CEP of the long driving laser pulse, and forward emission arises before the electron reflection. Only the emission at azimuthal angle  $\varphi = 0$  is shown.

The asymmetry parameter of these two peaks is shown to be CEP dependent and provides a sensitive measure of it. The designated regime is achieved in the relativistic domain, however, with a rather small Lorentz factor  $\gamma$  of the electrons, such that the interaction is below the, so-called, reflection condition  $\gamma \ll \xi$  [29,30]. Moreover, the stochasticity effects are required to be rather weak  $\chi \lesssim 0.1$  [31–33], opposite to the case considered in Ref. [34]. Here,  $\xi \equiv eE_0/(m\omega_0)$ ,  $E_0$  and  $\omega_0$  are the amplitude and frequency of the laser field, respectively, and  $-e$  and  $m$  the electron charge and mass, respectively;  $\chi \equiv |e|\sqrt{(F_{\mu\nu}p^\nu)^2}/m^3$  is the invariant quantum parameter [35,36],  $F_{\mu\nu}$  the field tensor, and  $p^\nu = (\epsilon, \mathbf{p})$  the incoming electron 4-momentum. Planck units  $\hbar = c = 1$  are used throughout.

In the common setup of nonlinear Compton scattering [29,37–40] the condition  $\gamma \gg \xi$  is employed, when the radiation concentrates in the forward direction relative to the initial motion of electrons. In the regime  $\gamma \sim \xi/2$ , backward emission appears [12,29,30,33,41,42]. When the laser and electron parameters are such that the reflection takes place at the peak of the laser pulse in the focal spot, a broad peak arises in the backward radiation [34]. In contrast to that in this Letter  $\gamma \ll \xi$ , when the electron is reflected before reaching the laser field peak and subsequently accelerated along the laser pulse. Before the reflection the forward radiation is weak due to the small  $\gamma$  and the low laser field. The electron radiates backwards after acceleration when it experiences the high gradient region of the laser pulse. Multiple backwards bursts of radiation correspond to the laser-cycle structure. While in the quantum regime of  $\chi \sim 1$  the multiple bursts coalesce into a single backward peak due to stochasticity effects of the photon emission [34], here for  $\chi \ll 1$  at least two backwards radiation peaks are well exhibited, see Fig. 2. These peaks sensitively probe the structure of the laser pulse. Consequently, the asymmetry of the peaks is significant even in the case of multicycle laser pulses. The asymmetry parameter of the peaks monotonically varies with respect to the CEP, allowing us to measure the CEP of multicycle laser pulses.

We employ a linearly polarized focused laser pulse with a Gaussian temporal profile, which propagates along  $+z$  direction and is polarized in  $x$  direction:  $\mathbf{E}(\mathbf{r}, \eta) \propto \exp[i(\eta + \psi_{\text{CEP}})] \exp(-\tau^2/T_0)$ , with the laser phase  $\phi = \eta + \psi_{\text{CEP}}$ ,  $\eta = \omega_0 t - k_0 z$ , and the CEP defined by  $\psi_{\text{CEP}}$ , see Refs. [43,44].  $\tau$  and  $T_0$  are the pulse and cycle duration, respectively, and,  $k_0$  is the laser wave vector. The peak intensity of the laser pulse is  $I \approx 4.9 \times 10^{23}$  W/cm<sup>2</sup> ( $\xi = 600$ ),  $\lambda_0 = 1$   $\mu\text{m}$ , and the beam waist is  $w_0 = 2$   $\mu\text{m}$ . The electron beam is assumed to be generated by the laser wakefield acceleration method [7,45–49], using a small fraction of the laser pulse to accelerate electrons. The initial mean kinetic energy of the electron is  $\epsilon_0 = 10$  MeV

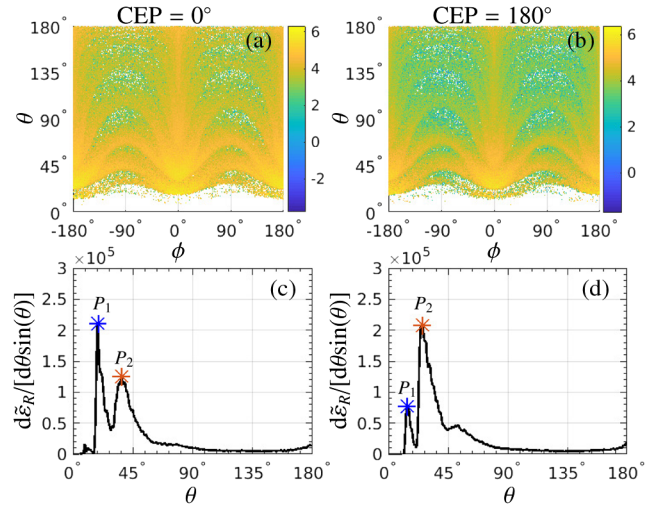


FIG. 2. (a),(b) Angle-resolved radiation energy  $\log_{10}[d\epsilon_R/d\Omega] \text{ rad}^{-2}$  in units of  $m$  vs the emission polar angle  $\theta$  and the azimuthal angle  $\phi$  ( $\Omega$  is the emission solid angle) in a 6-cycle laser pulse; the CEP  $\psi_{\text{CEP}} = 0^\circ$  and  $180^\circ$ , respectively. (c),(d)  $d\epsilon_R/[d\theta \sin(\theta)]$  vs  $\theta$ ;  $\psi_{\text{CEP}} = 0^\circ$  in (a),(c), and  $\psi_{\text{CEP}} = 180^\circ$  in (b),(d).  $P_1$  and  $P_2$  correspond to the two main peaks from left to right. All other parameters are given in the text.

( $\gamma_0 \approx 19.6$ , the maximum value of  $\chi$  during interaction  $\chi_{\text{max}} \approx 0.037$ ), and the energy and angular spread are  $\Delta\epsilon/\epsilon_0 = \Delta\theta = 0.02$ . The electron beam radius is  $w_e = \lambda_0$  and length  $L_e = 6\lambda_0$ , and the total electron number is  $N_e = 1.2 \times 10^5$  (electron density  $n_e \approx 6.37 \times 10^{15}$  cm<sup>-3</sup>). The electron radiation is simulated using the QED Monte Carlo approach, applicable in superstrong laser fields  $\xi \gg 1$  [43,50–52]. The photon emission probability in this limit is determined by the local value of the parameter  $\chi$  [53]. Between photon emissions, electrons are propagated via classical equations of motion.

The angular distributions of radiation in 6-cycle (FWHM) laser pulses with different CEPs are illustrated in Fig. 2. The laser and electron beam propagate with an initial polar angle  $\theta_L = 0^\circ$  and  $\theta_e = 179^\circ$ , respectively. In the considered linearly polarized laser pulse, the azimuthal angle  $\phi = 0^\circ$  and  $\pm 180^\circ$  correspond to the positive and negative directions of the polarization, respectively. The radiation around  $0^\circ$  and  $180^\circ$  is not symmetric due to the spatial asymmetry of the laser field.

The relativistic electrons penetrate into the laser field; however, the forward radiation is rather weak since the initial  $\chi \sim 10^{-2}$  is very small. As the electrons are reflected and accelerated by the intense laser field, the radiation which is in the backward direction relative to the electron initial motion, is enhanced. This is because the parameters  $\gamma$ ,  $\xi$ , and instantaneous emitted photon energy  $\epsilon_\gamma \sim \gamma\chi$  are increased. During the reflection, the emission polar angle  $\theta$  varies from  $180^\circ$  to close to  $0^\circ$ .

The angle-resolved spectra of the radiation significantly depend on the CEP. To quantify the CEP effect, we focus on

the strongest radiation domain along the polarization plane in the region of  $-15^\circ \leq \phi \leq +15^\circ$ , analyzing the radiation energy  $d\tilde{\epsilon}_R/[d\theta \sin(\theta)] = \int_{-15^\circ}^{+15^\circ} d\phi d\epsilon_R/d\Omega$ , as shown in Figs. 2(c) and 2(d). The two main peaks of the radiation are marked as  $P_1$  and  $P_2$ . The relative height of the peaks and the corresponding polar angles are different at  $\psi_{\text{CEP}} = 0^\circ$  and  $\psi_{\text{CEP}} = 180^\circ$ . We define the asymmetry parameter of the peaks  $\mathcal{A} = (M_{P_1} - M_{P_2})/(M_{P_1} + M_{P_2})$  with the height of the peaks  $M_{P_{1,2}} = d\tilde{\epsilon}_R/[d\theta \sin(\theta)]|_{\theta=\theta_{P_{1,2}}}$ , and the corresponding polar angles  $\theta_{P_1}$  and  $\theta_{P_2}$ , respectively.

We proceed with the analysis of the dependencies of  $\mathcal{A}$ ,  $\theta_{P_1}$ , and  $\theta_{P_2}$  on the CEP with a CEP interval of  $10^\circ$ , as shown in Fig. 3. And, the results of two laser intensities of  $I \sim 10^{22}$  W/cm $^2$  ( $\xi = 100$ ) and  $I \sim 10^{23}$  W/cm $^2$  ( $\xi = 600$ ) are compared.  $\mathcal{A}$ ,  $\theta_{P_1}$ , and  $\theta_{P_2}$  all monotonically increase with  $\psi_{\text{CEP}}$ , which can be used to characterize the CEP of the laser pulse. In particular, as shown in Fig. 3(a), the asymmetry parameter  $\mathcal{A}$  varies in a large range from approximately  $-0.5$  to  $0.5$  for both intensities. The emission angles of the peaks also can be used as a CEP indicator. As  $\theta_{P_2}$  varies with the CEP in a larger range than  $\theta_{P_1}$ , see Fig. 3(b) and (c) [ $\theta_{P_1}$  grows approximately by  $9.07^\circ$ , from  $12.81^\circ$  to  $21.88^\circ$ , for  $\xi = 600$ , and by  $10.1^\circ$ , from  $19.69^\circ$  to  $29.79^\circ$ , for  $\xi = 100$ ;  $\theta_{P_2}$  grows by  $20.4^\circ$ , from  $22.07^\circ$  to  $42.47^\circ$ , for  $\xi = 600$ , and by  $27.22^\circ$ , from  $31.4^\circ$  to  $58.62^\circ$ , for  $\xi = 100$ ], the determination of the CEP via  $\theta_{P_2}$  is preferable.

Note that the CEP signatures are not affected much from decreasing the value of the  $\chi$  parameter (for our calculations in the  $\xi = 100$  case the parameter  $\chi_{\text{max}} \approx 0.004$  is much smaller than  $\chi_{\text{max}} \approx 0.037$  for the  $\xi = 600$  case), although the total radiation intensity is decreased.

We analyze the emergence of radiation peaks and their relative heights in Fig. 4. Figures 4(a) and 4(b) show the radiation intensity resolved in laser cycles for  $\psi_{\text{CEP}} = 0^\circ$  and  $180^\circ$ , respectively. In each laser cycle the strongest

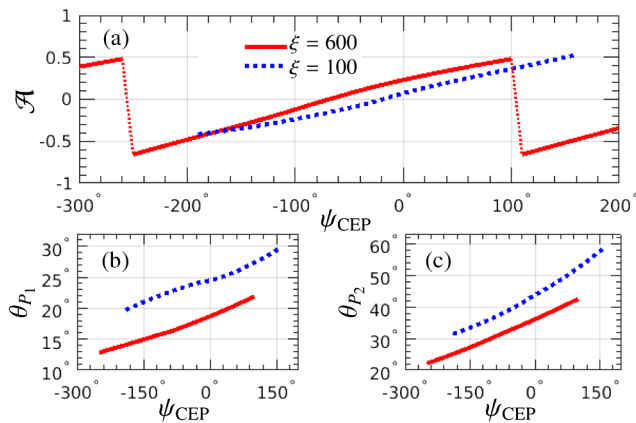


FIG. 3. (a) The asymmetry parameter  $\mathcal{A}$  of the backward radiation peaks  $P_1$  and  $P_2$  vs CEP. The polar angles (b)  $\theta_{P_1}$  and (c)  $\theta_{P_2}$  vs CEP. (red-solid lines)  $\xi = 600$ ,  $\epsilon_0 = 10$  MeV, (blue-dotted lines)  $\xi = 100$  and  $\epsilon_0 = 3$  MeV. The periodic variation of  $\mathcal{A}$  for  $\xi = 600$  is shown in (a), and is omitted for other cases. Other parameters are the same as in Fig. 2.

radiation arises near the peaks of the cycles at a certain emission angle. Between adjacent radiation peaks, there is a gap in the emission polar angle corresponding to the weak field part of the laser cycle. Integrating the radiation intensities in Figs. 4(a) and 4(b) by the emission laser phase  $\bar{\eta}$  generates the peak structures of radiation in Figs. 2(c) and 2(d). As the initial energies of the electrons  $\epsilon_0 \ll \xi/2$ , the electrons are easily reflected ( $\theta \approx 90^\circ$ ) and accelerated by the laser fields before the laser peak,  $\bar{\eta} \approx 5$  in Fig. 4(c), and  $\bar{\eta} \approx 4.2$  in Fig. 4(d). Shortly after the reflection, the ponderomotive force due to the transverse profile of the focused laser field pushes the electrons transversely out of the laser pulses [see the trajectories of the sample electrons in Figs. 4(g) and 4(h)]. The farther the electron is away from the

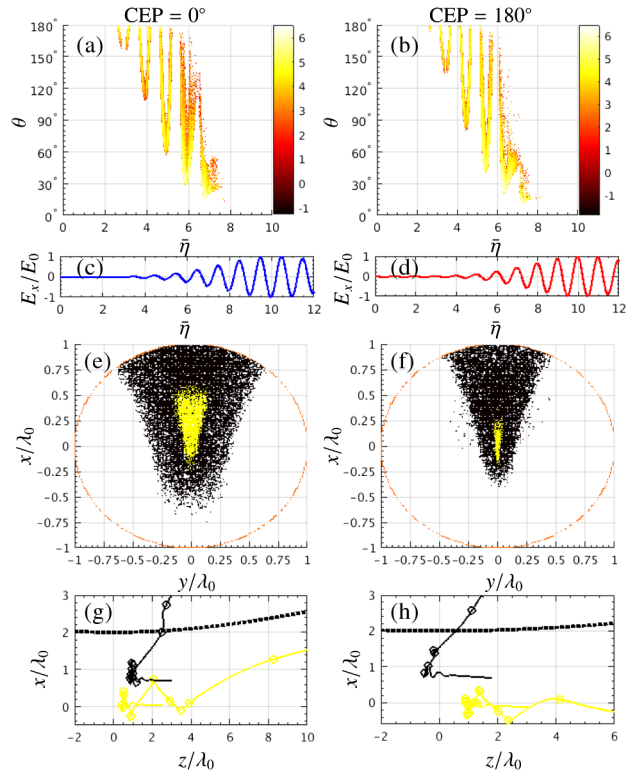


FIG. 4. Emergence of the radiation peaks  $P_1$ ,  $P_2$  (see Fig. 2): Left column is for  $\psi_{\text{CEP}} = 0^\circ$ , and right column for  $\psi_{\text{CEP}} = 180^\circ$ . (a),(b) Radiation intensity integrated over the azimuthal angle of  $-15^\circ \leq \phi \leq +15^\circ$ ,  $\log_{10}\{d^2\tilde{\epsilon}_R/[d\bar{\eta}d\theta \sin(\theta)]\}$ , vs emission phase  $\bar{\eta}$ , with  $\bar{\eta} = (\omega_0 t - k_0 z)/2\pi$ . (c),(d) The transverse component of electric fields  $E_x$  at the focus scaled by the laser amplitude  $E_0$  vs  $\bar{\eta}$ . (e),(f) The electron's initial spatial distribution in the cross section of the electron beam, which contributes to the spectral peak  $P_1$  (yellow only), and to the spectral peak  $P_2$  (black and yellow). The red circles show the boundary of the electron beam. (g),(h) Example trajectories of the electrons initially in the yellow region (yellow curves), and in the black region (outside of the yellow part, black curves), respectively. The photon emission is indicated by circles, and the dashed line shows the laser beam radius  $w_z = w_0 \sqrt{1 + (z/z_r)^2}$ . Other parameters are the same as in Fig. 2.

beam center, the faster it is expelled from the beam, and this at a larger angle. In fact, as illustrated in Figs. 4(e) and 4(f), the first peak  $P_1$  at small angles (Fig. 2) is exclusively formed by the radiation of the electrons initially located in the center of the beam (the yellow area of the beam), and the second peak  $P_2$  by the electrons located far from the beam center (the black and yellow areas). The reason is that the ponderomotive force, being proportional to the gradient of the transverse profile of the laser beam, is larger for electrons at the wings of the beam than in the center of the beam. Note, however, that during oscillation electrons from the yellow region radiate in other polar angles as well. Moreover, we find that the longitudinal position of the electron in the beam does not affect significantly the generation of radiation bursts. Note further that the whole interaction takes place mostly in the rising edge of the laser pulse, i.e., between  $\bar{\eta} \approx 3$  and  $\bar{\eta} \approx 7$ .

Let us estimate the resolution of our method for the CEP measurement. With current achievable angular resolution for x-ray registration in experiments of  $\approx 1$  mrad ( $\approx 0.057^\circ$ ) [54–56], the CEP can be measured via  $\theta_{P_2}$  ( $\theta_{P_2}$  changes by  $\approx 20^\circ$  within  $\Delta\psi_{\text{CEP}} = 360^\circ$  in Fig. 5) with an accuracy of approximately  $1^\circ$  in the case of a 6-cycle laser pulse. For the CEP retrieval with the asymmetry parameter  $\mathcal{A}$ , we estimate the feasible resolution of  $\mathcal{A}$  as  $\Delta\mathcal{A} \approx \Delta N_{\text{ph}}/N_{\text{ph}} \sim 1/\sqrt{N_{\text{ph}}}$  with the emitted photon number  $N_{\text{ph}}$ , and  $N_{\text{ph}} \approx \xi\alpha N_e$  [36], with the fine-structure constant  $\alpha$ , since the photon emission at  $P_{1,2}$  mainly happens during a single coherence length. In the considered electron beam with  $\xi = 100$ ,  $\Delta\mathcal{A} \approx 3.4 \times 10^{-3}$ , and the resolution of CEP detection is approximately  $1.2^\circ$ . With higher electron number  $N_e \sim 10^6$ , the CEP resolution improves to  $\sim 0.4^\circ$ .

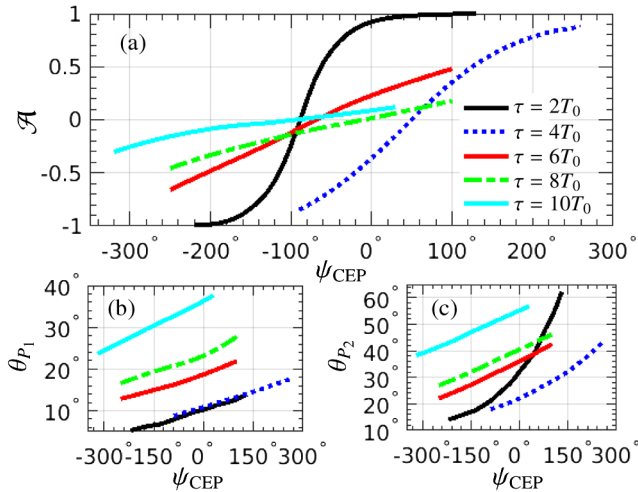


FIG. 5. The variations of (a)  $\mathcal{A}$  between  $P_1$  and  $P_2$  and the polar angles (b)  $\theta_{P_1}$  and (c)  $\theta_{P_2}$  with respect to the CEP. The black-solid, blue-dotted, red-solid, green-dash-dotted, and cyan-solid curves represent the cases of  $\tau = 2, 4, 6, 8,$  and  $10 T_0$ , respectively. Other parameters are the same as in Fig. 2.

The distinction of the present method of the CEP detection with respect to other methods [12,13] is that it is sensitive to CEP effects of relatively long laser pulses. The CEP signatures in dependence of the laser-pulse length are discussed in Fig. 5. As the laser-pulse duration increases from 2 cycles to 10 cycles, the gradient of the laser-field amplitude along the laser pulse decreases, and consequently, the gradient of  $\mathcal{A}$  as well, see Fig. 5(a). Although the gradient of the asymmetry parameter is large in the 2-cycle laser pulse in a certain CEP region, in the regions of  $\psi_{\text{CEP}} \lesssim -200^\circ$  and  $\psi_{\text{CEP}} \gtrsim 100^\circ$ ,  $\mathcal{A}$  saturates  $\mathcal{A} \approx \mp 1$ , when one of the peaks is much lower than the other. One can deduce from Fig. 5 that in ultrashort pulses less than 2 cycles,  $\theta_{P_1}$  becomes more suitable as a measure of the CEP because it maintains uniformity in the full CEP range. The CEP resolutions for the 4-, 6-, 8- and 10-cycle cases with other parameters as in Fig. 2 are approximately  $0.36^\circ, 0.44^\circ, 0.68^\circ,$  and  $0.93^\circ$ , respectively. Thus, the resolution is inversely proportional to the laser-pulse length. Meanwhile, the appropriate  $\gamma$  parameter should be at least one order of magnitude smaller than  $\xi$ . We also insured that the CEP signatures are rather insensitive to the electron-beam energy, energy spread, emittance, density, and length variations, as well as to the random phase of the laser prepulse [43].

Concluding, we investigated a new CEP effect of intense long laser pulses which arises in the ultrarelativistic regime of nonlinear Compton scattering. The field asymmetry in the rising edge of the laser pulse was shown to be responsible for the effect. In suitable conditions different parts of the electron beam are reflected, escape from the laser beam in different laser cycles, and generate two main peaks in backward direction. The asymmetry parameter and the corresponding emission polar angles of the two peaks can characterize the CEP of the laser pulse with a high resolution of about  $1^\circ$ , and the considered CEP signatures in this relativistic regime are very pronounced and observable in up to 10-cycle long laser pulses. The method is robust with respect to the laser and electron beam parameters and applies to currently achievable laser sources and those under construction of relativistic intensities.

Why should it be necessary to measure the CEP at full power? When a small fraction of the laser beam is extracted and the CEP measured, for instance, via the stereo-ATI [21], this provides the signature of the field's asymmetry near the peak of the laser pulse. Meanwhile, what is important for the ultrarelativistic interaction, is the asymmetry of the field in the rising edge of the laser pulse, and the concept for its measurement is provided here [43].

\*Jian-Xing.Li@mpi-hd.mpg.de

†k.hatsagortsyan@mpi-hd.mpg.de

[1] The Vulcan facility, <https://www.clf.stfc.ac.uk/Pages/The-Vulcan-10-Petawatt-Project.aspx>.

- [2] F. Negoita *et al.*, *Rom. Rep. Phys.* **68**, S37 (2016).
- [3] EII-Beamlines, <https://www.eli-beams.eu/en/facility/lasers/>.
- [4] Exawatt Center for Extreme Light Studies (XCELS), <http://www.xcels.iapras.ru/>.
- [5] M. Marklund and P. K. Shukla, *Rev. Mod. Phys.* **78**, 591 (2006).
- [6] G. A. Mourou, T. Tajima, and S. V. Bulanov, *Rev. Mod. Phys.* **78**, 309 (2006).
- [7] E. Esarey, C. B. Schroeder, and W. P. Leemans, *Rev. Mod. Phys.* **81**, 1229 (2009).
- [8] A. Di Piazza, C. Müller, K. Z. Hatsagortsyan, and C. H. Keitel, *Rev. Mod. Phys.* **84**, 1177 (2012).
- [9] G. Mourou and T. Tajima, *Eur. Phys. J. Spec. Top.* **223**, 979 (2014).
- [10] S. Meuren and A. Di Piazza, *Phys. Rev. Lett.* **107**, 260401 (2011).
- [11] M. Boca and V. Florescu, *Phys. Rev. A* **80**, 053403 (2009).
- [12] F. Mackenroth, A. Di Piazza, and C. H. Keitel, *Phys. Rev. Lett.* **105**, 063903 (2010).
- [13] D. Seipt and B. Kämpfer, *Phys. Rev. A* **88**, 012127 (2013).
- [14] F. Hebenstreit, R. Alkofer, G. V. Dunne, and H. Gies, *Phys. Rev. Lett.* **102**, 150404 (2009).
- [15] K. Krajewska and J. Z. Kamiński, *Phys. Rev. A* **86**, 052104 (2012).
- [16] N. Abdurkerim, Z.-L. Li, and B.-S. Xie, *Phys. Lett. B* **726**, 820 (2013).
- [17] A. I. Titov, B. Kämpfer, A. Hosaka, T. Nusch, and D. Seipt, *Phys. Rev. D* **93**, 045010 (2016).
- [18] M. J. A. Jansen and C. Müller, *Phys. Rev. D* **93**, 053011 (2016).
- [19] S. Meuren, C. H. Keitel, and A. Di Piazza, *Phys. Rev. D* **93**, 085028 (2016).
- [20] G. G. Paulus, F. Grasbon, H. Walther, P. Villoresi, M. Nisoli, S. Stagira, E. Priori, and S. De Silvestri, *Nature (London)* **414**, 182 (2001).
- [21] G. G. Paulus, F. Lindner, H. Walther, A. Baltuška, E. Goulielmakis, M. Lezius, and F. Krausz, *Phys. Rev. Lett.* **91**, 253004 (2003).
- [22] T. Wittmann, B. Horvath, W. Helml, M. G. Schatzel, X. Gu, A. L. Cavalieri, G. G. Paulus, and R. Kienberger, *Nat. Phys.* **5**, 357 (2009).
- [23] D. J. Jones, S. A. Diddams, J. K. Ranka, A. Stentz, R. S. Windeler, J. L. Hall, and S. T. Cundiff, *Science* **288**, 635 (2000).
- [24] X. Ren, A. M. Summers, K. R. Pandiri, A. Vajdi, V. Makhija, C. W. Fehrenbach, N. G. Kling, K. J. Betsch, Z. Wang, M. F. Kling, K. D. Carnes, I. Ben-Itzhak, C. Trallero-Herrero, and V. Kumarappan, *J. Opt.* **19**, 124017 (2017).
- [25] E. Goulielmakis, M. Uiberacker, R. Kienberger, A. Baltuska, V. Yakovlev, A. Scrinzi, T. Westerwalbesloh, U. Kleineberg, U. Heinzmann, M. Drescher, and F. Krausz, *Science* **305**, 1267 (2004).
- [26] M. Krefß, T. Löffler, M. D. Thomson, R. Dörner, H. Gimpel, K. Zrost, T. Ergler, R. Moshhammer, U. Morgner, J. Ullrich, and H. G. Roskos, *Nat. Phys.* **2**, 327 (2006).
- [27] V. Yanovsky, V. Chvykov, G. Kalinchenko, P. Rousseau, T. Planchon, T. Matsuoka, A. Maksimchuk, J. Nees, G. Cheriaux, G. Mourou, and K. Krushelnick, *Opt. Express* **16**, 2109 (2008).
- [28] F. Quéré, C. Thauray, J. P. Geindre, G. Bonnaud, P. Monot, and P. Martin, *Phys. Rev. Lett.* **100**, 095004 (2008).
- [29] P. Panek, J. Z. Kamiński, and F. Ehlötzky, *Phys. Rev. A* **65**, 022712 (2002).
- [30] F. Ehlötzky, J. Z. Kaminski, and K. Krajewskaa, *Rep. Prog. Phys.* **72**, 046401 (2009).
- [31] C. S. Shen and D. White, *Phys. Rev. Lett.* **28**, 455 (1972).
- [32] R. Duclous, J. G. Kirk, and A. R. Bell, *Plasma Phys. Controlled Fusion* **53**, 015009 (2011).
- [33] N. Neitz and A. Di Piazza, *Phys. Rev. Lett.* **111**, 054802 (2013).
- [34] J.-X. Li, Y.-Y. Chen, K. Z. Hatsagortsyan, and C. H. Keitel, *Sci. Rep.* **7**, 11556 (2017).
- [35] H. R. Reiss, *J. Math. Phys. (N.Y.)* **3**, 59 (1962).
- [36] V. I. Ritus, *J. Sov. Laser Res.* **6**, 497 (1985).
- [37] C. Bula, K. T. McDonald, E. J. Prebys, C. Bamber, S. Boege, T. Kotseroglou, A. C. Melissinos, D. D. Meyerhofer, W. Ragg, D. L. Burke, R. C. Field, G. Horton-Smith, A. C. Odian, J. E. Spencer, D. Walz, S. C. Berridge, W. M. Bugg, K. Shmakov, and A. W. Weidemann, *Phys. Rev. Lett.* **76**, 3116 (1996).
- [38] D. Seipt and B. Kämpfer, *Phys. Rev. A* **83**, 022101 (2011).
- [39] K. Krajewska, M. Twardy, and J. Z. Kamiński, *Phys. Rev. A* **89**, 052123 (2014).
- [40] M. Vranic, T. Grismayer, R. A. Fonseca, and L. O. Silva, *New J. Phys.* **18**, 073035 (2016).
- [41] A. Di Piazza, K. Z. Hatsagortsyan, and C. H. Keitel, *Phys. Rev. Lett.* **102**, 254802 (2009).
- [42] J.-X. Li, K. Z. Hatsagortsyan, B. J. Galow, and C. H. Keitel, *Phys. Rev. Lett.* **115**, 204801 (2015).
- [43] See the Supplemental Material at <http://link.aps.org/supplemental/10.1103/PhysRevLett.120.124803> for the details, which includes the employed electromagnetic fields of the laser pulse, the description of the applied methods for the calculation of the electron radiation, the roles of the laser and electron-beam parameters in the determination of the CEP, and the difference between the method provided in the Letter and the stereo-ATI approach.
- [44] Y. I. Salamin and C. H. Keitel, *Phys. Rev. Lett.* **88**, 095005 (2002).
- [45] B. Hidding *et al.*, *Phys. Rev. Lett.* **96**, 105004 (2006).
- [46] M. Mori *et al.*, *Phys. Rev. ST Accel. Beams* **12**, 082801 (2009).
- [47] A. Giulietti *et al.*, *Phys. Rev. Lett.* **101**, 105002 (2008).
- [48] L. M. Chen *et al.*, *Sci. Rep.* **3**, 1912 (2013).
- [49] B. S. Rao, A. Moorti, R. Rathore, J. A. Chakera, P. A. Naik, and P. D. Gupta, *Appl. Phys. Lett.* **102**, 231108 (2013).
- [50] N. V. Elkina, A. M. Fedotov, I. Y. Kostyukov, M. V. Legkov, N. B. Narozhny, E. N. Nerush, and H. Ruhl, *Phys. Rev. ST Accel. Beams* **14**, 054401 (2011).
- [51] C. P. Ridgers, J. G. Kirk, R. Duclous, T. G. Blackburn, C. S. Brady, K. Bennett, T. D. Arber, and A. R. Bell, *J. Comp. Physiol.* **260**, 273 (2014).
- [52] D. G. Green and C. N. Harvey, *Comput. Phys. Commun.* **192**, 313 (2015).
- [53] V. N. Baier, V. M. Katkov, and V. M. Strakhovenko, *Electromagnetic Processes at High Energies in Oriented Single Crystals* (World Scientific, Singapore, 1994).

- [54] A. Rousse, K. T. Phuoc, R. Shah, A. Pukhov, E. Lefebvre, V. Malka, S. Kiselev, F. Burgy, J.-P. Rousseau, D. Umstadter, and D. Hulin, *Phys. Rev. Lett.* **93**, 135005 (2004).
- [55] S. Cipiccia *et al.*, *Nat. Phys.* **7**, 867 (2011).
- [56] W. S. Graves, J. Bessuille, P. Brown, S. Carbajo, V. Dolgashev, K.-H. Hong, E. Ihloff, B. Khaykovich, H. Lin, K. Murari, E. A. Nanni, G. Resta, S. Tantawi, L. E. Zapata, F. X. Kärtner, and D. E. Moncton, *Phys. Rev. ST Accel. Beams* **17**, 120701 (2014).